Biosensors and Bioelectronics 25 (2010) 2436–2441

Contents lists available at ScienceDirect

Biosensors and Bioelectronics

journal homepage: www.elsevier.com/locate/bios

An excellent enzyme biosensor based on Sb-doped SnO_2 nanowires

Limiao Li[a,b], Jin Huang[b], Taihong Wang[b], Hao Zhang[a], Yang Liu[a], Jinghong Li[a,*]

[a] Department of Chemistry, Key Lab of Bioorganic Phosphorus Chemistry & Chemical Biology, Tsinghua University, Beijing 100084, China
[b] Key Laboratory for Micro-Nano Optoelectronic Devices of Ministry of Education, and State Key Laboratory for Chemo/Biosensing and Chemometrics, Hunan University, Changsha 410082, China

ARTICLE INFO

Article history:
Received 29 January 2010
Received in revised form 16 March 2010
Accepted 30 March 2010
Available online 7 April 2010

Keywords:
Doping
Semiconductor nanowire
Direct electrochemistry
Electrocatalysis
Biosensor

ABSTRACT

Sb-doped SnO_2 nanowires were synthesized via thermal evaporation. Scanning electron microscopic, transmission electron microscopic, X-ray diffraction, current–voltage, and electrochemical impedance spectroscopy experiments have been used to characterize the structural and electrical behaviors of the nanowires. A mediator-free horseradish peroxidase-based H_2O_2 biosensor was constructed through the Sb-doped SnO_2 nanowires used as the immobilization matrix for the enzymes. In comparison with the undoped SnO_2 nanowires, Sb-doped SnO_2 nanowires exhibited excellent electron transfer properties for the enzymes and higher electroactivity toward H_2O_2. The biosensors displayed good performance along with high sensitivity, wide linear range, and long-term stability. Those can be attributed to the enhanced carrier density arising from Sb doping and biocompatible microenvironment provided by the Sb-doped SnO_2 nanowires. This study demonstrated that Sb-doped SnO_2 nanowires were promising platform for the construction of mediator-free biosensors and provided new further fundamental insights into the study of nanoscience and nanodevices.

1. Introduction

Advances in nanotechnology and nanowires offer new directions in the design and development of electronic devices including field-effect transistors, detectors and light-emitting diodes, sensors, catalyst supports, solar cells, lithium ion batteries, environmental monitoring, and so on (Bruchez et al., 1998; Gan et al., 2004; Reis et al., 2006; Wen et al., 2009; Xia et al., 2003; Zhang et al., 2007). Owing to their dimensions in the range of 100 nm and high surface-to-volume ratios, nanowires display unique physical and chemical properties. Considerable attention has been paid to the application of nanowires in the bioanalysis and biosensors. The advantages such as aspect ratio, size scale, tunable electron transport, and other properties of nanowires are especially apparent in the construction of electrochemical sensors and biosensors based on one-dimensional (1-D) field-effect transistors (Chen et al., 2008; Cui et al., 2001; Wanekaya et al., 2006). In comparison with 2-D or 3-D structures where neighboring charges only influence on the surface, the charge effect in the nanowires takes place in the bulk of the structures. The surface-dominated properties of nanowires are highly sensitive to the local environment where neighboring charges could alter the overall electrical characters of nanowires (Hahm and Lieber, 2004; Li et al., 2004).

Electrochemical biosensors have been developed to be the most promising detection scheme owing to the advantages of simplicity, high reliability, sensitivity and selectivity, low cost, fast response, and ease of use (Liu et al., 2007; Lu et al., 2008; Kang et al., 2009; Yang et al., 2009). Nanowires with the unique catalytic activities and biocompatibility are widely used to improve the performance of electrochemical biosensors, such as decrease in overpotential, direct electron transfer capabilities, and high sensitivity and selectivity (Liu et al., 2006, 2009; Lu et al., 2007; Wang and Musameh, 2005; Zhang et al., 2008). These characteristics make the nanowire ideal substrate for the design of electrochemical biosensors. To achieve high-performance electrochemical biosensors, it is desired that the nanowires have the acceptable biocompatibility and good electrical properties. Therefore, nowadays, much interest has been focused on the development of new biocompatible and highly conductive nanowires for the biosensors. The modification of noble metal nanoparticle on the nanowire surface or the coat of biomimetic silica are effective approaches to improve the performance of biosensors due to the highly catalytic activity of noble metal and the high biocompatibility of silica matrix to maintain the nature characteristics of enzymes (Li and Lin, 2007; Ivnitski et al., 2008; Vamvakaki et al., 2008).

Semiconductor nanowires are widely investigated due to their special electrical and optical properties for the applications in the field of optoelectronics, sensors devices, solar conversion devices, and so on (Bao et al., 2007; Bharali et al., 2005; Kolmakov et al., 2006; Matthew and Song, 2009; Wang et al., 2006; Varghese et al., 2009). However, the low conductivity of semiconductor nanowires

* Corresponding author. Tel.: +86 10 62795290; fax: +86 10 62771149.
E-mail address: jhli@mail.tsinghua.edu.cn (J. Li).

0956-5663/$ – see front matter © 2010 Elsevier B.V. All rights reserved.
doi:10.1016/j.bios.2010.03.037

is not beneficial for the direct electron transfer and the construction of biosensors, which needs to be enhanced for the purpose to improve the performance of biosensors. The intentional incorporation of atomic impurities into semiconductor materials is a common routine for the purpose of tailoring properties such as band gap and electric conductivity to realize specific applications. Doping has proven to be an effective method to modulate the electric properties of semiconductor nanowires which has been well studied (Huang et al., 2007; Li et al., 2007; Luke et al., 2008; Wan et al., 2007, 2008).

In this paper, we firstly proposed the application of Sb-doped SnO_2 nanowire in the bioelectrochemistry. A mediator-free horseradish peroxidase (HRP) biosensor was constructed and exhibited good performance along with high sensitivity, wide linear range, and long-term stability. The results revealed that the immobilized HRP retained the bioactivity and simultaneously direct electron transfer of HRP was dramatically facilitated. In comparison with undoped SnO_2 nanowire, the Sb-doped SnO_2 nanowire exhibited excellent electron transfer properties for the enzymes and better ability to retain the electroactivity of enzymes. Our studies showed that Sb doping promoted direct electron transfer of the enzymes through the nanowires.

2. Experimental

2.1. Reagents

Sn and Sb powders were purchased from the Beijing Chemical Company. HRP was purchased from Beijing Dingguo Biotechnology Co. Ltd. All other chemical reagents used were of analytical grade without further purification. Phosphate buffer solution (PBS, pH 7.0, 0.1 M) was prepared with Na_2HPO_4 and KH_2PO_4. All solutions were prepared with doubly distilled water.

2.2. Synthesis of undoped and Sb-doped SnO_2 nanowires

The undoped and Sb-doped SnO_2 nanowires were synthesized by the thermal evaporation of Sn powders and mixed powders of Sn and Sb with the optimal weight ratio of 100:5, respectively. It is hardly to synthesize Sb-doped SnO_2 nanowires with high conductivity at lower weight ratio. The higher weight ratio will result in many impurities such as nanoparticles and nanosheets in the nanowires. The powders were located in an alumina boat, and the Si substrate covered with a thin Au film (10 nm) was placed on the top of the boat. The alumina boat was inserted into a horizontal furnace. The furnace was heated from room temperature to 800 °C and kept at this temperature for 1 h at the flow rate of 50 sccm N_2 gas. After the furnace was cooled down to room temperature, a layer of white product was obtained on the substrate.

2.3. Characterization

X-ray diffraction (XRD) was performed in the 2θ range from 20° to 60° on a Bruker D8-Advance X-ray powder diffractometer with monochromatized Cu Kα radiation. The scanning electron microscopic (SEM) image was carried out by Hitachi 4200 (Hitachi, Japan). The transmission electron microscopic (TEM) image was performed on JEM 2010 high-resolution transmission electron microscope opened at an accelerating voltage of 120 kV. UV–vis absorption spectroscopy was done by a UV-2100S spectrophotometer (Shimadzu).

2.4. Electrical measurement

The current–voltage curves were obtained through the measurement of FET where the nanowires acted as the channel materials. The fabrication procedure of FET was described as follows: Before the fabrication of the devices, the Si substrate used was sonicated in the acetone, ethanol and pure water. Poly(methyl methacrylate) (PMMA) in chlorobenzene was spin-coated onto the substrate, and then annealed at 180 °C for 1 h. The undoped and Sb-doped SnO_2 nanowires were transferred from the growth substrate to the PMMA layer through a physical transfer method. The nanowires-coated template substrate and the device substrate were put into the probe station. The tungsten mechanical probe tips precisely controlled by probe manipulators penetrated through the PMMA layer to pick up single SnO_2 nanowire via the electrostatic force and then transferred it to the device substrate coated with 300 nm SiO_2 layer. The whole process was observed under a high-magnification optical microscope. Finally, highly conductive ITO source and drain electrodes with the thickness of 100 nm were deposited by rf magnetron sputtering in pure argon ambient at 0.5 Pa. The electrical transport measurements were performed with a semiconductor parameter characterization system (Keithley 4200 SCS) and a Micromanipulator probe station in a clean and shielded box at room temperature in air ambient. The morphology of the devices was examined by high-magnification optical microscope (Olympus, Japan).

2.5. Electrochemical measurements

Prior to the electrode modification, the glassy carbon (GC) electrodes were polished with 1.0, 0.3, and 0.05 μm alumina powder, and then sonicated in ethanol and water, each for 2 min. The modified electrodes were prepared by a simple casting method. Typically, 8 μL of nanowires (1 mg/mL, ethanol) suspension was mixed with 8 μL of HRP (2 mg/mL, 0.1 M PBS, pH 7.0) solution. Then, 6 μL of the mixed dispersion was cast onto the GC electrode. After dried at room temperature, the modified electrodes were stored at 4 °C in refrigerator. Electrochemical experiments were performed at room temperature on a CHI 660B electrochemical station (CHI Instruments Inc., USA) with a conventional three-electrode system. The nanowire modified GC electrode and Ag/AgCl (saturated KCl) electrode were used as the working and reference electrodes, respectively. The Pt wire acted as the counter electrode. The buffer solutions were purged with highly purified nitrogen gas for at least 30 min prior to the electrochemical experiments. The impedance measurements were performed in the presence of 5 mM $[Fe(CN)_6]^{3-/4-}$ in 0.1 M KCl from 10 kHz to 0.1 Hz at an ac amplitude of 10 mV under a bias potential of 300 mV condition.

3. Results and discussion

3.1. Characterizations of Sb-doped SnO_2 nanowire

The structural and morphological characters of nanowires were obtained by XRD, SEM and TEM analysis, as shown in Fig. 1. Fig. 1(A) is the XRD spectrum of Sb-doped SnO_2 nanowires. All reflections of the nanowires are in excellent accordance with a tetragonal rutile structure. The peak with the label * is owing to the Si substrate. The diffraction peaks are similar to those of undoped SnO_2 nanowires. No peaks of other impurities, such as Sb or Sb_2O_5, are detected. The SEM image is given in Fig. 1(B). The average diameter of Sb-doped SnO_2 nanowires is about 100 nm. The Sb doping has no influence on the morphological characters of the nanowires. At the bottom of the nanowires, Au particles are observed, which indicates that the growth mechanism is Au-catalyzed vapor–liquid–solid mode. The Sb atoms are *in situ* doped into SnO_2 nanowires during the growth process. The thermal evaporation method can well maintain the crystal matrix integrity of Sb-doped SnO_2 nanowire. Fig. 1(C) and (D) shows the high resolution TEM images of the Sb-doped SnO_2

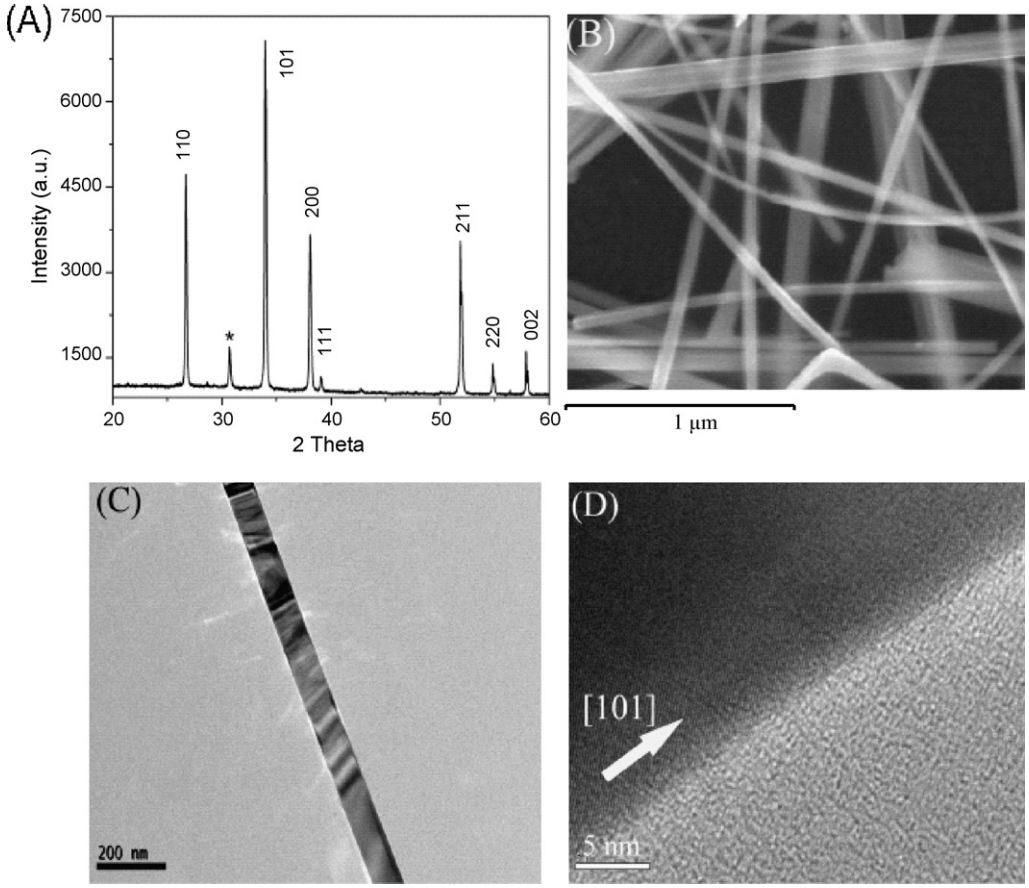

Fig. 1. XRD pattern (a), SEM image (b), and TEM images (c and d) of Sb-doped SnO_2 nanowires.

nanowires, which confirm that the Sb-doped SnO_2 nanowires are single-crystalline phases.

3.2. Current–voltage curves of Sb-doped SnO_2 nanowires

The optical image of the device is shown in the inset of Fig. 2 in which a single SnO_2 nanowire connects two ITO electrodes. The distance between the two electrodes is 80 μm. Fig. 2 exhibits the typical current–voltage curves of undoped and Sb-doped SnO_2 nanowires at room temperature in air ambient. The resistivity of undoped SnO_2 nanowire was about 12.73 Ω cm. For comparison, the resistivity of Sb-doped SnO_2 nanowire was decreased to be 4.13×10^{-3} Ω cm. The increased conductivity confirmed that Sb atoms were successfully doped into SnO_2 nanowires and greatly enhanced the carrier concentration.

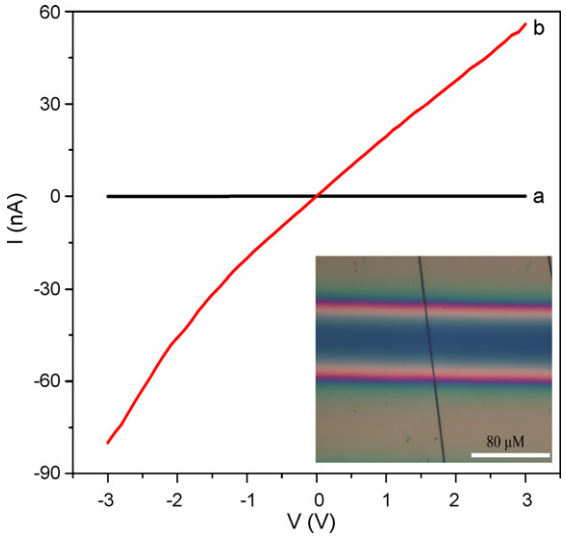

Fig. 2. Typical characteristics of *I–V* curves of undoped (a) and Sb-doped (b) SnO_2 nanowires as the voltage is scanned from −3 to 3 V. Inset: optical image of our device.

3.3. Electrochemical impedance response of Sb-doped SnO_2 nanowires

As is well known, electrochemical impedance spectroscopy (EIS) is an effective method to investigate the change of interface properties of an electrode surface in the modified process. Fig. S1 shows the results of the EIS at undoped SnO_2 nanowire/GC electrode (a) and Sb-doped SnO_2 nanowire/GC electrode (b) in the presence of 5 mM $[Fe(CN)_6]^{3-/4-}$ in 0.1 M KCl (see supporting information). The impedance spectra consist of a semicircular domain that corresponds to the electron transfer-limited process, and a straight line that related to diffusion controlled process. To understand clearly the electrical properties of the prepared electrode/solution interfaces, the equivalent circuit was chosen to fit the EIS results, as shown in the inset of Fig. S1. R_s was the solution-phase resistance and was identical during the experiments. Other elements in the equivalent circuit were shown as follows: R_{ct}, charge transfer resistance; CPE, constant phase element; and Z_W, the Warburg impedance. The semicircle diameter equals R_{ct}, which exhibits the electron transfer kinetics of the redox-probe at the electrode interface. The R_{ct} was about 28 kΩ for undoped SnO_2 nanowire/GC electrode. It is clearly observed that a much lower charge transfer resistance for $[Fe(CN)_6]^{3-/4-}$

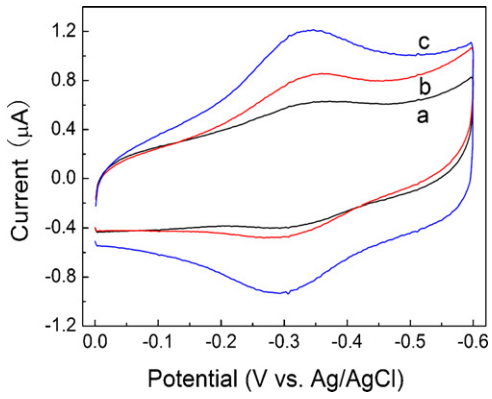

Fig. 3. Cyclic voltammograms of HRP on bare (a), SnO_2 nanowire (b) and Sb-doped SnO_2 nanowire (c) modified glassy carbon electrodes in 0.1 M PBS (pH 7.0) at the scan rate of 100 mV/s.

at Sb-doped SnO_2 nanowire/GC electrode, indicating that better reversibility of electrode reaction and faster electron transfer at the Sb-doped SnO_2 nanowire/GC electrode surface. The superior properties of Sb-doped SnO_2 nanowire/GC electrode are believed to be ascribed to the Sb doping, which greatly enhances the carrier concentration and facilitates the charge transfer through the surface. Therefore, the Sb-doped SnO_2 nanowires provide an ideal substrate to study the redox properties of redox proteins.

3.4. HRP/Sb-doped SnO_2 nanowire hybrid film

The SEM image of HRP/Sb-doped SnO_2 nanowire hybrid film on GC electrode surface shows that Sb-doped SnO_2 nanowires are packed densely but do not lay flat, resulting in a rough surface (Fig. S2). The rough surface is generally beneficial in increasing the sensitivity of an amperometric biosensor. The HRP nanoparticles appeared as white dots can be observed from the inset. They are absorbed on the surface of nanowires or trapped between them, which can prevent the leakage of enzymes during electrochemical measurement. As it is known that the immobilization of enzyme on a solid surface can cause some native conformation change or denaturation in some cases, UV–vis absorption spectra are used to study the influence of nanowires on the structural feature of enzymes. The UV–vis spectra of free HRP, HRP/undoped SnO_2 nanowire and HRP/Sb-doped SnO_2 nanowire hybrids with the same enzyme concentration are shown in Fig. S3 (see supporting information). The Soret band position of the HRP immobilized in Sb-doped SnO_2 nanowires is located at 405 nm, which is quite similar to those of the free HRP, suggesting that the enzyme molecules retain their native structures after hybrid with the nanowires.

3.5. Electron transfer of HRP/Sb-doped SnO_2 nanowire electrode

We further studied the electrochemical properties of the modified electrodes of HRP immobilized on different substrates. Fig. 3 shows cyclic voltammograms (CVs) of HRP (a), HRP/SnO_2 nanowires (b) and HRP/Sb-doped SnO_2 nanowires (c) modified GC electrodes in N_2-saturated PBS. Comparing to those obtained at bare and HRP/SnO_2 nanowires modified GC electrodes, remarkably larger peak currents were obtained at the HRP/Sb-doped SnO_2 nanowires modified GC electrode. In addition, a pair of well-defined redox peaks at HRP/Sb-doped SnO_2 nanowires modified GC electrode was observed. The formal potential (E^0) calculated by averaging the cathodic and anodic peak potentials is −0.327 V. According to Faraday's law, $Q = nFA\Gamma^*$, where F is Faraday's constant, A is the geometrical surface area of the electrode, n is the number of electron transferred and Q is the charge by integrating the cathodic peak of HRP at the CV, the surface concentration of electroactive HRP (Γ^*) at the Sb-doped SnO_2 nanowires/HRP modified GC electrode was estimated to be 3.36×10^{-9} mol cm^{-2} by assuming a one-electron transfer reaction. This value is higher than those of HRP at bare (5.91×10^{-10} mol cm^{-2}) and SnO_2 nanowires/HRP modified GC electrodes (8.06×10^{-10} mol cm^{-2}). Accordingly, the Sb-doped SnO_2 nanowires-based electrode presented a much higher surface concentration of electroactive HRP than that of electrode without Sb doping. Here, it should be noted that the electrodes of HRP immobilized on both undoped and Sb-doped SnO_2 nanowires modified GC electrodes were fabricated under the same conditions. The only difference between them was of the Sb doping. As a result, the higher current response and larger concentration of electroactive HRP should be associated with the Sb doping effect on the SnO_2 nanowires.

The CVs of HRP/Sb-doped SnO_2 nanowires modified GC electrode at various scan rates were shown in Fig. S4(A) (see supporting information). Both the cathodic and the anodic peak currents increased with the scan rate and enhancements of both currents are linear to the increase of scan rate as shown in Fig. S4(B). The facts indicated that the redox process of HRP on the Sb-doped SnO_2 nanowire modified electrodes was a reversible and surface-confined process. It is known that the active redox center of HRP is deeply embedded in a protective protein shell, which makes the direct electron transfer between the enzymes and the electrodes extremely difficult. An important feature for the immobilized enzyme electrode lies in that the active substrate layer can improve the electron transfer ability between the enzyme and electrode surface. Therefore, the electrochemical performance of the immobilized enzyme electrode is also largely dependent on the electrochemical properties of the active layer on the electrode. In our system, the doping of Sb could enhance both the conductivity and the carrier concentration of the SnO_2 nanowires, which can improve the electron transfer between the HRP and the GC electrode surface.

3.6. Electrocatalysis of H_2O_2 at HRP/Sb-doped SnO_2 nanowires

The electrocatalytic performances of the HRP/Sb-doped SnO_2 nanowires modified GC electrode were investigated. Fig. 4 shows the CVs of HRP/Sb-doped SnO_2 nanowires modified GC electrode in the absence (a) and presence of 10 μM (b), 50 μM (c) and 100 μM (d) of H_2O_2 at the scan rate of 100 mV/s. When H_2O_2 was added into the PBS, the voltammetric behavior of the modified electrode changed dramatically. The reduction peak current at −0.32 V showed an obvious increase, whereas the oxidation peak current disappeared due to the fast electron transfer between the HRP and

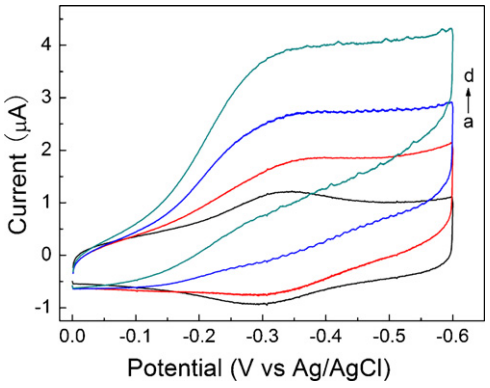

Fig. 4. Cyclic voltammograms of HRP/Sb-doped SnO_2 nanowires modified glassy carbon electrode in 0.1 M PBS (pH 7.0) in the absence (a) and presence of 10 μM (b), 50 μM (c) and 100 μM (d) H_2O_2 at the scan rate of 100 mV/s.

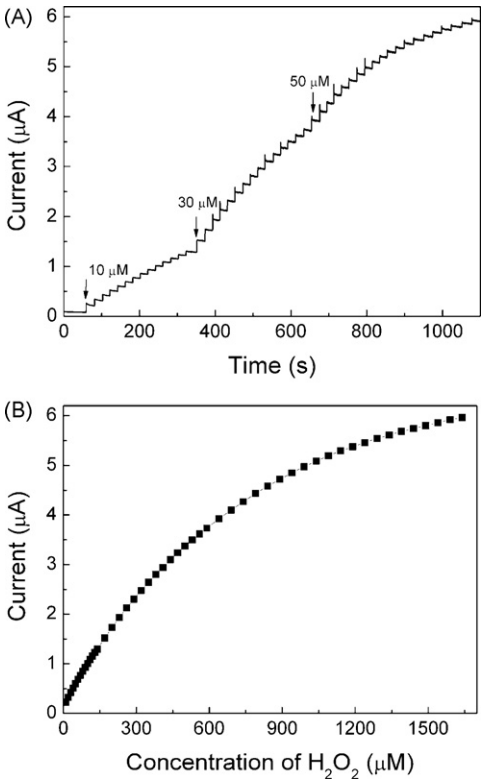

Fig. 5. (A) Amperometric response of Sb-doped SnO_2/HRP modified glassy carbon electrode to H_2O_2 in 0.1 M PBS (pH 7.0) at −0.3 V vs. Ag/AgCl (sat. KCl). (B) The corresponding calibration curve between the current response and concentration of H_2O_2.

H_2O_2. These results indicated that the immobilized HRP enzymes effectively retained their electrocatalytic activity toward the reduction of H_2O_2.

The amperometric response of the HRP/Sb-doped SnO_2 nanowires modified GC electrode was performed through successive addition of H_2O_2 into a continuously stirred buffer solution at the potential of −0.3 V, as shown in Fig. 5(A). After the addition of H_2O_2, the current immediately increased and reached 95% of the steady state value within ~5 s, showing a fast response. Fig. 5(B) illustrates the dependence of the electrocatalytic current on the concentration of H_2O_2. A linear relationship between the current and the concentration was established in the concentration range from 10 to 450 μM (R = 0.994), and a sensitivity of 100 mA M^{-1} cm^{-2} was obtained from the slope in the linear range. The detection limit is 0.8 μM at a signal-to-noise ratio of 3. The low detection limit, superior sensitivity and fast response can be ascribed to the rapid electron transfer between HRP and the doped nanowires modified electrode, and the highly electroactive properties of the immobilized HRP. The Michaelis–Menten constant K_m was calculated to be 0.76 mM according to the Lineweaver–Burk equation (Kamin and Wilson, 1980).

In order to provide further insight into the nature of the increased electrochemical and enzymatic response of the HRP/Sb-doped SnO_2 nanowire, the current response of HRP in PBS with various concentrations of H_2O_2 at bare (a), HRP/SnO_2 nanowires (b), and HRP/Sb-doped SnO_2 nanowires (c) modified GC electrodes were performed at the same potential, as shown in Fig. 6. Repetitive measurements were carried out in 50 μM H_2O_2 solution. For the bare, HRP/SnO_2 nanowires, and HRP/Sb-doped SnO_2 nanowires modified GC electrodes, the results of 10 successive amperometric measurements showed a relative standard deviation of 4.2, 3.8, and 3.63%. It shows that the current response of the HRP/Sb-doped SnO_2

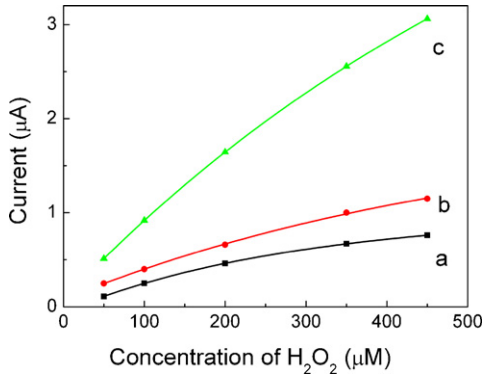

Fig. 6. Calibration curves of HRP (a), HRP/undoped SnO_2 nanowires (b), and HRP/Sb-doped SnO_2 nanowires (c) modified glassy carbon electrodes. The applied potential is −0.3 V vs. Ag/AgCl (sat. KCl).

nanowires electrode is much larger than those of HRP immobilized on bare and SnO_2 nanowires modified GC electrodes. Moreover, the slope of the calibration curve on the HRP/Sb-doped SnO_2 nanowires electrode is larger than others, exhibiting its higher sensitivity. In an electrocatalytic process of enzymatic reaction, the current response is dependent upon enzyme activity and the electron transfer rate between the enzyme and electrode surface.

In our system, for the enzyme immobilized on the active substrate layer, the electron transfer process of an electrocatalytic reaction includes four steps: (1) electron transfer between the substrate and enzyme, (2) electron transfer between enzyme and the nanowires, (3) electron transportation in the nanowires, (4) electron transfer between the nanowires and electrode surface. In the step 1, electron transfer rate is dependent on the intrinsical properties of enzyme. While in other steps, it is related with the electrochemical properties of the active layer on electrode. The enhanced electrocatalytic response of HRP/Sb-doped SnO_2 nanowires modified GC electrode suggests that Sb doping leads to the increase in the wiring efficiency of the enzymes and electron transport through the hybrid film.

3.7. *Stability of HRP/Sb-doped SnO_2 nanowires modified GC electrode*

The stability of the HRP/Sb-doped SnO_2 nanowires modified GC electrode was performed by measuring the current response of the hybrid electrode in PBS (pH 7.0) with 50 μM of H_2O_2. The response of HRP/Sb-doped SnO_2 nanowire modified GC electrode can retain 95.3% of its original signal after 10 days storage. For comparison, the stability of HRP/SnO_2 nanowire modified GC electrode and HRP modified GC electrode were also explored under the same situation; they kept 90 and 55% of their initial response current after 10 days, suggesting that the stability of HRP/Sb-doped SnO_2 nanowire modified GC electrode is nearly equivalent to that of HRP/SnO_2 nanowire modified GC electrode but is far better than that of HRP modified GC electrode. The better stability of HRP/Sb-doped SnO_2 nanowire modified GC electrode may be attributed to the excellent biocompatibility of Sb-doped SnO_2 nanowires that offered a favorable microenvironment to the immobilized HRP. After 1 month storage, 89% of its initial activity can be obtained.

4. Conclusions

In summary, this study has a new insight to investigate the doping of semiconductor nanowires effect on the electrochemical properties of immobilized HRP. Direct electron transfer between HRP and the electrode was obtained on the Sb-doped SnO_2 nanowires modified GC electrode. The electron transfer rate and

the ability to retain the electroactivity of HRP are better than that of undoped SnO_2 nanowire modified GC electrode due to Sb doping. Moreover, the HRP/Sb-doped SnO_2 nanowires modified GC electrode exhibited low detection limit, wide linear range, fast response, high sensitivity and excellent stability for the detection of H_2O_2. Therefore, the outstanding electrocatalytic properties together with high biocompatibility make the Sb-doped SnO_2 nanowires an interesting candidate for the study of electrochemistry behaviors of proteins as well as sensing applications.

Acknowledgements

This work was financially supported by the National Natural Science Foundation of China (No. 20975060) and National Basic Research Program of China (No. 2007CB310500).

Appendix A. Supplementary data

Supplementary data associated with this article can be found, in the online version, at doi:10.1016/j.bios.2010.03.037.

References

Bao, J., Chen, W., Liu, T.T., Zhu, Y.L., Jin, P.Y., Wang, L.Y., Liu, J.F., Wei, Y.G., Li, Y.D., 2007. ACS Nano 1, 293–298.
Bharali, D.J., Lucey, D.W., Jaykumar, H., Pudavar, H.E., Prasad, P.N., 2005. J. Am. Chem. Soc. 127, 11364–11371.
Bruchez, M., Moronne, M., Gin, P., Weiss, S., Alivisatos, A.P., 1998. Science 281, 2013–2016.
Chen, C.P., Ganguly, A., Wang, C.H., Hsu, C.W., Chattopadhyay, S., Hsu, Y.K., Chang, Y.C., Chen, K.H., Chen, L.C., 2008. Anal. Chem. 81, 36–42.
Cui, Y., Wei, Q., Park, H., Lieber, C.M., 2001. Science 293, 1289–1292.
Gan, X., Liu, T., Zhong, J., Liu, X.J., Li, G., 2004. Chem. Biol. Chem. 5, 1686–1691.
Hahm, J., Lieber, C.M., 2004. Nano Lett. 4, 51–54.
Huang, J., Lu, A.X., Zhao, B., Wan, Q., 2007. Appl. Phys. Lett. 91, 073102-1-3.
Ivnitski, D., Artyushkova, K., Rincn, R.A., Atanassov, P., Luckarift, H.R., Johnson, G.R., 2008. Small 4, 357–364.
Kamin, R.A., Wilson, G.S., 1980. Anal. Chem. 52, 1198–1205.
Kang, X.H., Wang, J., Wu, H., Aksay, I.A., Liu, J., Lin, Y.H., 2009. Biosens. Bioelectron. 25, 901–905.
Kolmakov, A., Klenov, D.O., Lilach, Y., Stemmer, S., Moskovits, M., 2006. Nano Lett. 6, 667–673.
Li, J., Lin, X.Q., 2007. Biosens. Bioelectron. 22, 2898–2905.
Li, L.M., Li, C.C., Zhang, J., Du, Z.F., Zou, Z.F., Yu, H.C., Wang, Y.G., Wang, T.H., 2007. Nanotechnology 18, 225504.
Li, Z., Chen, Y., Li, X., Kamins, T.I., Nauka, K., Williams, R.S., 2004. Nano Lett. 4, 245–247.
Liu, A., Wei, M.D., Honma, I., Zhou, H., 2006. Adv. Funct. Mater. 16, 371–376.
Liu, J.P., Guo, C.X., Li, C.M., Li, Y.Y., Chi, Q.B., Huang, X.T., Liao, L., Yu, T., 2009. Electrochem. Commun. 11, 202–204.
Liu, Q., Lu, X.B., Li, J., Yao, X., Li, J.H., 2007. Biosens. Bioelectron. 22, 3203–3209.
Lu, X.B., Zhou, J.H., Lu, W., Liu, Q., Li, J.H., 2008. Biosens. Bioelectron. 23, 1236–1243.
Lu, Y.S., Yang, M.H., Qu, F.L., Shen, G.L., Yu, R.Q., 2007. Bioelectrochemistry 71, 211–218.
Luke, T.L., Wolcott, A., Xu, L.P., Chen, S.W., Wen, Z.H., Li, J.H., Rosa, E.D.L., Zhang, J.Z., 2008. J. Phys. Chem. C 112, 1282–1292.
Matthew, J., Song, J., 2009. Energy Environ. Sci. 2, 1050–1059.
Reis, C.P., Nenfeld, R.J., Ribeiro, A.J., Veiga, F., 2006. Nanomedicine 2, 53–65.
Varghese, O.K., Paulose, M., LaTempa, T.J., Grimes, C.A., 2009. Nano Lett. 9, 731–737.
Vamvakaki, V., Hatzimarinaki, M., Chaniotakis, N., 2008. Anal. Chem. 80, 5970–5975.
Wan, Q., Dattoli, E.N., Lu, W., 2007. Appl. Phys. Lett. 90, 222107.
Wan, Q., Dattoli, E., Lu, W., 2008. Small 4, 451–454.
Wanekaya, A.K., Chen, W., Myung, N.V., Mulchandani, A., 2006. Electroanalysis 18, 533–550.
Wang, J., Musameh, M., 2005. Anal. Clim. Acta 539, 209–213.
Wang, X., Zhou, J., Liu, J., Xu, N., Wang, Z.L., 2006. Nano Lett. 6, 2768–2772.
Wen, Z.H., Ci, S.Q., Li, J.H., 2009. J. Phys. Chem. C 113, 13482–13487.
Xia, Y.N., Yang, P.D., Sun, Y.G., Wu, Y.Y., Mayers, B., Gates, B., Yin, Y.D., Kim, F., Yan, H.Q., 2003. Adv. Mater. 15, 353–389.
Yang, S., Jia, W.Z., Qian, Q.Y., Zhou, Y.G., Xia, X.H., 2009. Anal. Chem. 81, 3478–3484.
Zhang, Q., Zhang, L., Li, J.H., 2007. J. Phys. Chem. C 111, 8655–8660.
Zhang, X.Y., Li, D., Bourgeois, L., Wang, H.T., Webley, P.A., 2008. Chem. Phys. Chem. 10, 436–441.